1-2021

A New Line-By-Line Methodology Based on the Spectral Contributions of the Bands

Felipe R. Coelho
Federal University of Rio Grande do Sul

Aline Ziemniczak
Federal University of Rio Grande do Sul

Somesh Roy
Marquette University, somesh.roy@marquette.edu

Francis H.R. França
Federal University of Rio Grande do Sul

International Journal of Heat and Mass Transfer, Vol. 164 (January 2021): 120423. DOI.

A New Line-By-Line Methodology Based on the Spectral Contributions of the Bands

Felipe R. Coelho
Department of Mechanical Engineering, Federal University of Rio Grande do Sul, Porto Alegre, RS, Brazil
Aline Ziemniczak
Department of Mechanical Engineering, Federal University of Rio Grande do Sul, Porto Alegre, RS, Brazil
Somesh P. Roy
Department of Mechanical Engineering, Marquette University, Milwaukee WI
Francis H.R. França
Department of Mechanical Engineering, Federal University of Rio Grande do Sul, Porto Alegre, RS, Brazil

Abstract

This study presents a new methodology to solve thermal radiation in participating gases, the spectrally reduced integration (SRI), which employs a non-uniform spectral discretization to considerably reduce the computational

cost of the line-by-line (LBL) solution while still maintaining good levels of accuracy. This non-uniform spectral mesh is generated from discretization schemes based on the spectral contributions of the bands, which apply less or more refined spectral resolution depending on the importance of the bands to the radiative transfer. Based on this methodology, several schemes were initially proposed and evaluated for a homogeneous H_2O-CO_2 mixture test case. Results showed that the most refined schemes were able to generate highly accurate results three to five times faster than the reference LBL solution, while the coarser schemes were still interesting alternatives for faster but still reliable calculations. In fact, a compromise between the accuracy of the SRI solution and the total number of spectral intervals was observed in all the tested schemes. The SRI method also presented similarly promising results when solving non-homogeneous test cases. Finally, the present study also develops two alternatives to address the need of a priori evaluation of the spectral contributions of the bands when using the discretization schemes. These two methodologies produced surprisingly accurate solutions of the non-homogeneous test cases, each with its own advantages and disadvantages, and could be applied together to further simplify the use of the SRI in highly accurate coupled combustion problems.

Keywords

Thermal radiation, Line-by-line, Spectrally reduced integration, Discretization schemes, Spectral contributions of the bands

1. Introduction

The ever severe environmental restrictions motivate researchers to continuously seek higher efficiency and lower flue gas emissions in combustion applications. In order to achieve that, accurate modeling of all the involved physical phenomena is needed. This includes thermal radiation, which is often the dominant heat transfer mechanism in combustion due to the high temperatures resulted from the chemical reactions [1]. Furthermore, reaction products such as CO_2, H_2O, and soot act as participating media in the radiative transfer, which increases significantly the complexity of the problem. Another difficulty of modeling thermal radiation in combustion is that: since it affects the temperature field, it also affects the chemical kinetics and soot formation [2]. These changes in the combustion dynamics then have a feedback on the radiative transfer, requiring a coupled solution of these complex phenomena.

The radiative heat transfer in participating media is modeled through the radiative transfer equation (RTE), which describes the attenuation and augmentation of the spectral radiation intensity along the domain [1], [3]. The solution of the RTE is complex since it requires spatial, directional, and spectral integration. The spectral integration is particularly challenging, mainly due to the highly irregular wavenumber dependence of the absorption coefficient of participating gases. This erratic behavior results from the sum of contributions of millions of spectral lines that compose the absorption spectrum of the gas. To further complicate the problem, the absorption spectrum is also a function of the thermodynamic state of the medium, which usually varies considerably along the domain in real combustion scenarios.

The most accurate methodology of spectral integration of the RTE is the line-by-line (LBL) method, which considers the contribution of all the relevant spectral lines individually for the absorption coefficient calculation. However, because of the highly irregular wavenumber dependence of the absorption spectrum, this integration is often performed with a very fine spectral resolution, which results in prohibitively high computational cost. This is especially problematic in three dimensional combustion-coupled simulations, in which thermal radiation is only one part of the solution [1]. Due to this limitation, radiation in participant gases is more commonly solved using approximate spectral models, which significantly simplifies the spectral integration of the RTE, and LBL calculations are mainly limited to benchmark solutions of relatively simpler uncoupled problems.

In recent years, the most commonly employed spectral models for participating gases are the narrow band models [4], [5], [6] and global models such as the weighted-sum-of-gray-gases (WSGG) [7], [8], [9], the spectral-line-based WSGG (SLW) [10], [11], and the full-spectrum k-distribution (FSK) [12], [13], [14]. One of the most active areas of research is testing and evaluating the accuracy of these models against benchmark LBL solutions. In particular, some studies perform a detailed analysis of the LBL parameters for 1 atm [7], [8], while others extend this discussion to higher total pressures [9], [10], [15]. In general, the WSGG model has shown satisfactory results when compared to the LBL, especially when considering its low computational cost [7], [9]. On the other hand, the narrow band models are able to produce benchmark levels of accuracy [4], [5], [6], but at the cost of a higher CPU time. The SLW and FSK are in between the two previous spectral models, resulting in good accuracy [10], [14], [16] at a moderate solution speed.

Despite its high computational cost, the LBL method was used in heat transfer solutions already in earlier studies [17], [18], [19]. In particular, the work from [17] computed the absorption spectrum for a spectral resolution of 0.01 cm^{-1}, but ended up having to smooth it by a factor of 10 in order to achieve viable solution times back then. Chu et al. [20] claimed that a uniform spectral resolution of 0.02 cm^{-1} is adequate for atmospheric total pressure LBL solutions, while the use of lower resolutions would lead to results with considerable deviations. These recommendations were then used in [15], [21]. An even finer discretization of 0.005 cm^{-1} was utilized by Pearson et al. [10], perhaps due to the sub-atmospheric total pressures conditions, which are known to require higher wavenumber resolutions [1], [22]. On the other hand, Dorigon et al. [7] performed a spectral grid analysis in terms of total emittance values, concluding that a wavenumber resolution of 0.067 cm^{-1} would be enough for 1 atm. In a more recent study, Ziemniczak et al. [23] managed to considerably smooth the LBL spectral discretization through a reduction technique, decreasing its computational cost while maintaining satisfactory accuracy. This same reduction methodology was also used by Rodrigues et al. [24], calling it the direct spectral integration (DSI) of the RTE, to obtain reference solutions that could be used to distinguish the deviations introduced by different variations of the WSGG model against laminar non-premixed flames experimental data. The main motivation behind the use of the DSI in that study was to avoid the very high CPU demands of the LBL integration in a commercial CFD software [24].

In contrast to these limitations of the standard LBL method in coupled combustion solutions, the LBL Monte Carlo method is a promising alternative for more advanced problems and became extensively studied in recent years [25], [26], [27], [28], [29], [30], [31]. Since the ray tracing of the Monte Carlo method is already CPU intensive by itself, using the LBL to treat the spectral lines behavior does not drastically increase the computational cost of the solution [1]. Another significant advantage of the method over traditional LBL solvers is that, through spectral random-number relations, it chooses the wavenumbers of emission based on their contributions to the energy emitted [25], [28], [29]. However, this advantage does not necessarily need to be limited to the Monte Carlo as the LBL method could also base its spectral discretization on the contributions of each wavenumber to the radiative heat transfer. In fact, instead of using a uniform spectral smoothing technique such as the ones used by the DSI [23], [24], employing a non-uniform reduction based on the spectral contributions of the bands should considerably improve accuracy of the method.

Therefore, as an attempt to improve the efficiency of the LBL integration, this study proposes the spectrally reduced integration (SRI) method, which employs non-uniform spectral discretizations based on the spectral contributions of the bands to considerably decrease the computational cost of the solution. Since the RTE results of most interest are usually the radiative heat flux and source term, the contributions are based on these quantities instead of the fraction of energy emitted that is employed on the wavenumber relations of the Monte Carlo method. To the authors' best knowledge, there is still no study that proposes a line-by-line methodology that utilizes non-uniform spectral discretizations based on the contributions of the bands to the radiative heat

flux and source term. Furthermore, independent studies show that these contributions can behave considerably different than the emission contributions.

The main objective of this study is to present the SRI method and develop reliable non-uniform discretization schemes based on the spectral contributions of the bands to the radiative heat flux and source term. These discretization schemes considerably lower the number of spectral intervals while maintaining accurate solutions. The reduction of the wavenumber mesh is performed through a similar technique as the one employed in the DSI [23], [24], yet the SRI allows variable levels of refinement depending on the importance of each region of the spectrum to the radiative transfer. Thus, the SRI is more suited to benchmark solutions for which a standard LBL solution is not computationally viable, and presents a better compromise between accuracy and computational cost than the DSI. Another major objective of this study is to develop methodologies that address the need of a priori evaluation of the spectral contributions before generating discretization schemes for different problems. Finally, this study also analyzes how the different configurations of discretization schemes compare to each other when applied to the same problem, evaluating the compromise between accuracy and computational cost.

2. Methodology

2.1. Absorption coefficient calculation

When soot particles are not present, the main participating species among the combustion products are usually CO_2 and H_2O. Since the spectral behavior of the absorption coefficient of soot is considerably smoother than those of molecular gases [1], studying a gas mixture composed of only CO_2 and H_2O is enough for the purpose of this work. The absorption coefficient κ_η for this gas mixture is then obtained through

(1)

$$\kappa_\eta = \kappa_{\eta,\mathrm{c}} + \kappa_{\eta,\mathrm{w}}$$

where $\kappa_{\eta,\mathrm{c}}$ and $\kappa_{\eta,\mathrm{w}}$ are the absorption coefficients of the individual gases CO_2 and H_2O, respectively. These single species absorption coefficients are calculated through

(2)

$$\kappa_{\eta,i}(\eta, p, T, Y_i) = N(p,T) Y_i C_{\eta,i}(\eta, p, T, Y_i)$$

in which N is the gas molar density and $\kappa_{\eta,i}$, Y_i and $C_{\eta,i}$ are, respectively, the absorption coefficient, the mole fraction and the absorption cross-section of species i. Since this study only considers a mixture composed of two gases, the index i can be either equal to c, which stands CO_2, or w, which stands for H_2O. To obtain the absorption cross-sections of the individual gases CO_2 and H_2O, the Lorentz profile is employed, such that

(3)

$$C_\eta = \sum_{k=1}^{K} C_{\eta,k} = \sum_{k=1}^{K} \frac{S_k}{\pi} \frac{\gamma_k}{{\gamma_k}^2 + (\eta - \eta_k)^2}$$

where K is the total number of significant spectral lines, k is the index of the spectral line, $C_{\eta,k}$ is the contribution of the spectral line to the absorption cross-section, S_k is the integrated line intensity, γ_k is the line half-width of the line profile, and η_k is the wavenumber location of the center of the spectral line. The Lorentz profile considers that the main reason for spectral line broadening is the collision between the molecules of the gas,

which is regarded as the dominant broadening mechanism in most engineering applications [1], [3]. As an alternative, the Voigt profile is a more general line shape, including both collision and Doppler broadening of the spectral lines. However, independent studies and results from Wang and Modest [22] indicate that, for the conditions studied in this work, the difference between the profiles is negligible.

In principle, all the absorption lines of the spectrum should be included in Eq. (3). However, $C_{\eta,k}$ of the lines rapidly decreases as the wavenumbers move away from the line center position η_k, the contributions of this line *k* become negligible after a certain range. Thus, in order to avoid excessive computational time when generating new absorption spectra, most authors cut the line profile after this region, commonly known as the line wing cutoff [10], [32]. This limit is usually defined as a fixed wavenumber interval [5], [7] or a variable wavenumber interval based on a certain number of line half-widths γ_k [10], [15], [20], [32]. For instance, the study from Dorigon et al., [7] employed fixed $\Delta\eta_{cut} = 40\ \mathrm{cm}^{-1}$ for H_2O, while the study from Pearson et al. [10] utilized $\Delta\eta_{cut} = 2750\gamma_k$ for this same gas. When comparing these methodologies, the one based on the line half-widths has two considerable advantages. The first one is that γ_k and, consequently, the broadening of each line *k*, varies considerably from line to line, such that defining a fixed value might be inefficient for lines that present low levels of broadening. The second advantage is that the parameter γ_k also incorporates thermodynamic state dependence of the line wings. Therefore, the present study employed line wing cutoffs based on the line half-widths, such that $\Delta\eta_{cut,c} = 30000\gamma_k$ for CO_2 and $\Delta\eta_{cut,w} = 3000\gamma_k$ for H_2O. Independent analyses showed that doubling these values of cutoff only changed the results of radiative heat flux and source term by 0.02% and 0.01%, respectively. Furthermore, these values are very conservative, being higher than the ones in [10], [32], especially for CO_2, and significantly higher than the value of $20\gamma_k$ used in [15], [20].

The line half-width γ_k was calculated using the high-resolution spectroscopic database HITEMP2010 [33], such that

(4)

$$\gamma_k = \left(\frac{T_{ref}}{T}\right)^{n_i}\left(p_i\gamma_{self,k} + (p - p_i)\gamma_{air,k}\right)$$

in which $T_{ref} = 296$ K is the reference temperature of the HITEMP2010, n_i is the temperature dependence coefficient, p_i is the partial pressure of species *i*, $\gamma_{self,k}$ is the line self-broadening, and $\gamma_{air,k}$ is the broadening caused by air. The integrated line intensity S_k is given by Rothman et al. [33]

(5)

$$S_k(T) = S_k(T_{ref})\frac{Q(T_{ref})}{Q(T)}\frac{\exp(-C_2E_k/T)}{\exp(-C_2E_k/T_{ref})}\frac{[1 - \exp(-C_2\nu_k/T)]}{[1 - \exp(-C_2\nu_k/T_{ref})]}$$

where *Q* is the total internal partition sum, E_k is the energy of the lower state, and ν_k is the energy difference between the initial and final state. The remaining line parameters η_k, n_i, $\gamma_{self,k}$, $\gamma_{air,k}$, $S_k(T_{ref})$, *Q*, E_k, and ν_k from Eqs. (3)–(5) were taken from the high resolution spectroscopic database HITEMP2010 [33].

Using the described methodology, the absorption cross-sections were calculated for mole fractions of $Y_c = 1$ for CO_2 and $Y_w = 0.01$, 0.1, 0.2 for H_2O, temperatures ranging from 300 K to 2500 K, and total pressure of 1 atm. The temperature range was divided in intervals of 100 K, while the intermediate values were calculated through linear interpolation. The mole fractions of H_2O were chosen to cover the ranges of $0 \leq Y_w \leq 0.2$, which are around typical concentrations in stoichiometric air methane combustion applications. Linear interpolation is used to calculate intermediate absorption cross-section values. Although the ranges of interest for CO_2 would be near

$0 \leq Y_c \leq 0.1$ in such scenarios, due to its negligible self-broadening effect [34], only a single value of Y_c is needed. The wavenumber range considered for the absorption spectra is from 0 cm^{-1} to 10000 cm^{-1}. Complementary results showed that, for the thermodynamic conditions considered in this study, increasing this spectral domain had negligible effects on the LBL solutions. Through a detailed spectral grid analysis presented in Section 2.2, discretizations consisting of 150 000 division were found to be adequate for 1 atm.

2.2. Line-by-line (LBL) integration of the RTE

All the problems solved in this study consist of a one-dimensional slab, in which the participating medium is contained between two parallel black walls. These cases also consider mixtures of only CO_2 and H_2O, with no soot, where neglecting the scattering effect is a good approximation. For a nonscattering medium, the RTE results from the local balance between emission and absorpion along a certain pathway, such that [1], [3]

(6)

$$\frac{dI_\eta}{ds} = -\kappa_\eta I_\eta + \kappa_\eta I_{b\eta}$$

where I_η is the spectral radiation intensity, $I_{b\eta}$ the blackbody spectral radiation intensity, and s is the path length. Applying the discrete ordinates method (DOM) for the angular discretization of Eq. (6) and simplifying it for a one-dimensional problem in direction x, results in

(7)

$$\mu_l \frac{dI^+_{\eta,l}}{dx} = -\kappa_\eta I^+_{\eta,l} + \kappa_\eta I_{b\eta}$$

(8)

$$-\mu_l \frac{dI^-_{\eta,l}}{dx} = -\kappa_\eta I^-_{\eta,l} + \kappa_\eta I_{b\eta}$$

in which μ_l are the direction cosines of the angles ϑ_l, ϑ_l is the angle between the x direction and the $I^+_{\eta,l}$ or $I^-_{\eta,l}$ directions l, and $I^+_{\eta,l}$ and $I^+_{\eta,l}$ are, respectively, the spectral radiation intensity for $\mu_l > 0$ and $\mu_l < 0$. A schematic of this one-dimensional problem, illustrating the presented variables, is shown in Fig. 1, where the length L is the distance between the black walls.

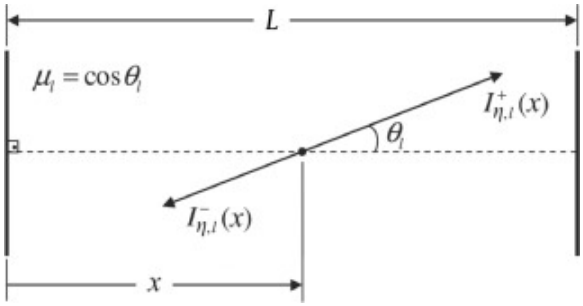

Fig. 1. Schematic of the one-dimensional slab problem (Adapted from Dorigon et al. [7]).

Since the walls are assumed to be black, the boundary conditions for Eqs. (7) and (8) are $I^+_{\eta,l}(0) = I_{b\eta}(0)$,, for the left wall at $x = 0$, and $I^-_{\eta,l}(L) = I_{b\eta}(L)$,, for the right wall at $x = L$. Using these boundary conditions to

solve Eqs. (7) and (8) for both $I^+_{\eta,l}$ and $I^-_{\eta,l}$ and balancing out these spectral radiative intensities for all the *l* directions, the local radiative heat flux q_r and radiative source term S_r can be calculated by

(9)

$$q_r(x) = \int_\eta \sum_{l=1}^{n_d} [2\pi\mu_l w_l (I^+_{\eta,l}(x) - I^-_{\eta,l}(x))]\, d\eta$$

(10)

$$S_r(x) = \int_\eta \{\sum_{l=1}^{n_d} [2\pi\kappa_\eta w_l (I^+_{\eta,l}(x) - I^-_{\eta,l}(x))] - 4\pi\kappa_\eta I_{b\eta}\}\, d\eta$$

where w_l is the quadrature weight for *l* direction and n_d is the total number of directions. In this study, the Gauss-Legendre quadrature was used and the quadrature weights w_l considered that

(11)

$$\sum_{l=1}^{n_d} w_l = 1$$

The numerical evaluation of Eqs. (9) and (10) was performed for nd=15 directions, which resulted in a total of 30 directions for the DOM, while the distance *L* was divided in 200 uniform intervals Δ*x*, resulting in nx=201 points. Independent studies showed that these levels of angular and spatial discretization were enough for the one-dimensional problems studied here. For the spectral discretization, $n_p = 150000$ spectral points between 0 cm^{-1} to 10 000 cm^{-1}, resulting in $\Delta\eta = 0.0667\ \mathrm{cm}^{-1}$, have been shown to be enough for atmospheric total pressure conditions [7], [23]. However, some authors claimed that a spectral resolution of $\Delta\eta = 0.02\ \mathrm{cm}^{-1}$ was required to avoid considerable deviations [15], [20], [21], while some employed even finer resolutions [8], [10].

Since the main goal of the present study is to increase the efficiency of the LBL calculations, starting from a reference LBL solution that presents higher computational cost than necessary is not interesting. Therefore, a spectral grid analysis for a one-dimensional problem at 1 atm was performed, considering five different wavenumber meshes: $n_p =$ 37 500, 75 000, 150 000, 250 000 and 500 000. The case, named Case 1, consists of a uniform mixture of H_2O and CO_2 with $Y_w = 0.2$ and $Y_c = 0.1$ and at 2500 K. These chosen values of temperature and mole fractions are the maximum values considered in this study, which makes them the critical conditions for the calculation of the radiative heat flux and source term. Furthermore, the walls are at 300 K and the distance between them is chosen as $L = 1$ m. This wavenumber grid analysis was performed in terms of the maximum values of the radiative heat flux and source term along the domain, which, in Case 1, are both located right next to the walls where the temperature abruptly changes from 300 K to 2500 K.

The results for the maximum radiative heat flux and source term as a function of the number of spectral intervals n_p for Case 1 are presented in Fig. 2. This figure shows that an almost asymptotic behavior was observed from $n_p = 250\ 000$ onward. Independent studies show that the behavior of the curves become truly asymptotic from $n_p = 1\ 000\ 000$ onward, while the deviations between the meshes are lower than 0.01% for higher spectral resolutions. Nonetheless, the spectral resolution of $n_p = 150\ 000$ was chosen as the reference solution in this study, mainly for two reasons. The first one is that Case 1 considers the highest temperature of

2500 K along the whole domain, which is a critical condition since the collision broadening reduces with temperature, as can be seen in Eq. (4). When the broadening and, consequently, the overlap between different lines reduces, a finer resolution is needed to capture the highly irregular behavior of absorption spectrum [22]. The second reason is that, even if high accuracy in such an extreme case was needed, despite the resolution of $n_p = 150\,000$ being out of the asymptotic zone of grid independence from Fig. 2, it resulted in relative deviations of only 0.02% for radiative heat flux and 0.1% for radiative source term when compared to the most refined discretization of $n_p = 500\,000$. This means that a reference solution employing $n_p = 150\,000$ was accurate enough, and that increasing it to $n_p = 250\,000$ would probably not be worth the higher computational time, especially when considering that the main objective of this study is to improve the efficiency of the LBL method. Moreover, the conclusions of the present analysis are in agreement with the ones from [7], [23], showing that 150 000 spectral intervals were enough to generate accurate LBL solutions even at high temperatures such as 2500 K. In spite of this, it was also shown that, if a strict spectral grid independence was desired, a resolution of $n_p = 250\,000$ or even $n_p = 500\,000$ might be needed, which is not far off from what was recommended in [15], [20], [21].

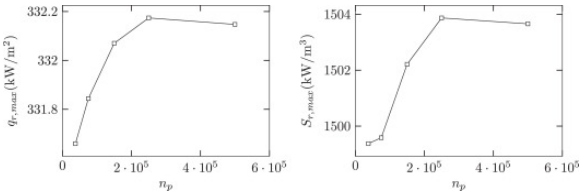

Fig. 2. Spectral grid analysis for Case 1 in terms of the maximum radiative heat flux and source term.

2.3. Spectral contributions of the bands

In heat transfer problems, it is usually required to determine the total radiative heat flux and source term, that is, after integrating these quantities in the whole spectrum, as presented in Eqs. (9) and (10). However, since this study is interested in the contribution of each spectral interval $\Delta\eta$, working with the spectral radiative heat flux and source term is more convenient, which are given by

(12)

$$q_{r,\eta}(\eta, x) = \sum_{l=1}^{n_d} [2\pi\mu_l\omega_l(I_{\eta,l}^{+}(x) - I_{\eta,l}^{-}(x))]$$

(13)

$$S_{r,\eta}(\eta, x) = \sum_{l=1}^{n_d} [2\pi\kappa_\eta\omega_l(I_{\eta,l}^{+}(x) - I_{\eta,l}^{-}(x))] - 4\pi\kappa_\eta I_{b\eta}$$

It is important to notice that both the spectral radiative heat flux and source term are still functions of *x* and can assume positive or negative values along the domain. In fact, this means that each spectral interval $\Delta\eta$ can contribute to increase or decrease the integrated quantities.

This analysis seeks a non-uniform spectral discretization that is based on these spectral contributions, but the wavenumber intervals are meant to be constant in the *x* direction. A good alternative of a spectral contribution that considers the spatial dependence but is not a function of *x* would be to obtain mean values of the spectral radiative heat flux and source term along the domain. Nonetheless, to avoid negative contributions canceling

out positive contributions in other *x* positions, these averages need to be performed in terms of absolute values of $q_{r,\eta}$ and $S_{r,\eta}$, such that

(14)

$$\zeta_{q_r}(\eta) = \frac{1}{L}\int_0^L |q_{r,\eta}(\eta, x)|\, dx$$

(15)

$$\zeta_{S_r}(\eta) = \frac{1}{L}\int_0^L |S_{r,\eta}(\eta, x)|\, dx$$

where ζ_{q_r} and ζ_{S_r} are the spectral contributions of each spectral interval $\Delta\eta$ for the radiative heat flux and source term, respectively. In this study, the integrals from Eqs. (14) and (15) were solved numerically and, since the the *x* domain was divided in uniform intervals Δx, it resulted in a simple arithmetic mean in the *x* direction. Furthermore, due to this spatial integration, the contribution of each band becomes a global variable of the domain. This enables a fixed spectral discretization, but it may lead to the limitation of being restricted to a specific problem or, at least, problems very similar to the one from where ζ_{q_r} and ζ_{S_r} were obtained. In fact, investigating the possibility of generalizing these results to similar conditions is one of the goals of this study.

The parameters ζ_{q_r} and ζ_{S_r} can be interpreted as the mean absolute contribution along the domain of a certain spectral band to the radiative heat flux and source term. Since the average is performed in terms of the absolute values, both the contributions to absorption and emission of a certain band are included in ζ_{q_r} and ζ_{S_r}. For example, one band might have a large contribution to the absorption in the cold regions of the gas, resulting in a positive $S_{r,\eta}$ in that *x* position, while also contributing to the emission in the hot regions of the gas, which would result in a negative $S_{r,\eta}$ in that *x* position. After performing this average of the absolute values, the resulting physical units of ζ_{q_r} and ζ_{S_r} are the same as $q_{r,\eta}$ and $S_{r,\eta}$, respectively. However, having dimensionless spectral contributions would be more useful since it allows the direct comparison between ζ_{q_r} and ζ_{S_r} and also between the spectral contributions of different problems. In order to achieve that, ζ_{q_r} and ζ_{S_r} are divided by their maximum values along the spectrum, such that

(16)

$$\zeta^*_{q_r}(\eta) = \frac{\zeta_{q_r}(\eta)}{\zeta_{q_r,max}}$$

(17)

$$\zeta^*_{S_r}(\eta) = \frac{\zeta_{S_r}(\eta)}{\zeta_{S_r,max}}$$

in which $\zeta^*_{q_r}$ and $\zeta^*_{S_r}$ are, respectively, the dimensionless spectral contributions of bands to the radiative heat flux and source term, while $\zeta_{q_r,max}$ and $\zeta_{S_r,max}$ are, respectively, the maximum values in the entire spectrum.

To illustrate how $\zeta^*_{q_r}$ and $\zeta^*_{S_r}$ vary along the spectrum, a first example of the spectral contributions for a homogeneous H_2O-CO_2 mixture, with $Y_w = 2Y_c = 0.2$, in non-uniform temperature conditions, given by $T(x) = 300\text{K} + 2200\text{K}\sin^2(\pi x)$, is shown in Fig. 3(a), for the spectral resolution of 150 000 points. As can be seen, for this spectral discretization, both the contributions $\zeta^*_{q_r}$ and $\zeta^*_{S_r}$ present a highly irregular wavenumber

dependence, similar to what is observed in the spectral absorption coefficient. In fact, the fluctuations are so intense that it is hard to distinguish which bands influence the results the most. Moreover, the contributions of the spectral intervals oscillate so fast along the spectrum that defining a less refined discretization scheme seems impracticable. Nonetheless, despite this highly irregular behavior of the contributions, it is evident from the picture that the spectral contributions of a band to the radiative heat flux and source term are somewhat different.

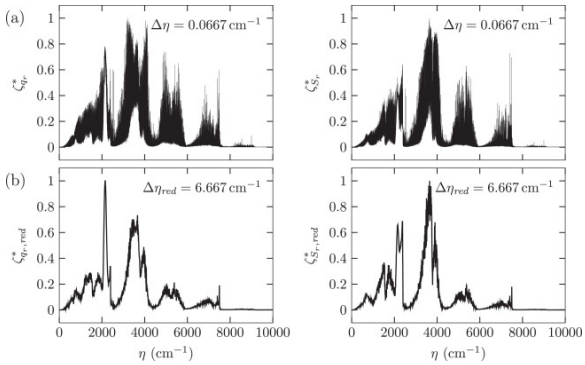

Fig. 3. Spectral contributions of the bands to the radiative heat flux and source term for a first example when considering (a) $\Delta\eta = 0.0667\ \mathrm{cm}^{-1}$ and (b) $\Delta\eta_{red} = 6.667\ \mathrm{cm}^{-1}$.

To allow better visualization of the importance of the spectral bands and enable the generation of less refined discretization schemes, a reduction methodology is applied to the contributions $\zeta^*_{q_r}$ and $\zeta^*_{S_r}$. This reduction technique consists of performing means of $\zeta^*_{q_r}$ and $\zeta^*_{S_r}$ in the wavenumber η inside spectral intervals $\Delta\eta_{red} = 100\Delta\eta = 6.6667\ \mathrm{cm}^{-1}$. This lowers the spectral resolution of $\zeta^*_{q_r}$ and $\zeta^*_{S_r}$ by a reduction sample of $n_{red} = 100$, resulting in a total of 1500 η_{red} points. Two higher values, $n_{red} = 200$ and 400, and two lower values, $n_{red} = 25$and50, were also evaluated. Although the differences were small, $n_{red} = 100$ still resulted in slightly lower deviations. However, it is important to clarify that this value of $n_{red} = 100$ is by no means an optimal value; even if it was, it would only be an optimal value for this specific problem. Considering such methodology, the expressions for the spectral contributions of the first reduced band $\Delta\eta_{red}$ are given by

(18)

$$\zeta^*_{q_r,red} = \frac{1}{\Delta\eta_{red}} \int_{\Delta\eta_{red}} \zeta^*_{q_r} d\eta$$

(19)

$$\zeta^*_{S_r,red} = \frac{1}{\Delta\eta_{red}} \int_{\Delta\eta_{red}} \zeta^*_{S_r} d\eta$$

where $\zeta^*_{q_r,red,}$ and $\zeta^*_{S_r,red}$ are, respectively, the reduced spectral contributions to the radiative heat flux and source term. This methodology is very similar to the one employed by Ziemniczak et al. [23] and Rodrigues et al. [24], except for the fact that the reduction technique in this analysis is only applied to the final results of $\zeta^*_{q_r}$ and $\zeta^*_{S_r}$, while the absorption coefficient, spectral radiative heat flux and source term are still evaluated for the original 150 000 wavenumber points.

The results for this spectrally reduced $\zeta^*_{q_r,red}$ and $\zeta^*_{S_r,red}$ as a function of the wavenumber η for this first example are also shown in Fig. 3(b). According to this figure, after the reduction methodology, a clearer definition of the

most important bands for the radiative heat flux and source term is attained. Furthermore, it is interesting to see that, even after the spectral reduction, $\zeta^*_{q_r,red}$ and $\zeta^*_{S_r,red}$ distributions are indeed different. These results can now be used to generate non-uniform spectral discretizations, employing a finer mesh on the bands that contribute the most and a coarser mesh on those not as important. Taking $\zeta^*_{q_r,red}$ and $\zeta^*_{S_r,red}$ from Fig. 3 as an example, the stronger bands near 2150 cm^{-1} and 3600 cm^{-1} would require a great level of refinement, probably equal to the reference LBL solution, while some bands present almost negligible contributions, such as the ones from 7600 cm^{-1} onward. A detailed analysis on the importance of each band and the spectral discretization they required is performed in this study, from case to case.

2.4. Spectrally reduced integration (SRI) of the RTE

The spectrally reduced integration (SRI) method solves the RTE from Eq. (6) in a similar manner as the LBL method, but employing a non-uniform wavenumber mesh with lower resolution than the one from the reference solution. In this study, the SRI method also performs numerical calculations of the Eqs. (9) and (10) using the same spatial and angular discretizations as the LBL solution. On the other hand, the spectral discretization of the SRI is a function of the chosen discretization scheme, which generates the non-uniform wavenumber mesh based on the reduced contributions of the bands. This is performed through the usage of discretization groups, which define different spectral reduction samples for each of the desired ranges of $\zeta^*_{q_r,red}$ and $\zeta^*_{S_r,red}$. These reductions are then applied to the absorption cross-sections of both H_2O and CO_2, similarly to the methodologies from [23], [24], resulting in

(20)

$$C_{\eta,red,j} = \frac{1}{\Delta\eta_{red,j}} \int_{\Delta\eta_{red,j}} C_\eta d\eta$$

where $C_{\eta,red,j}$ is the absorption cross-section which is spectrally reduced by the discretization group j and $\Delta\eta_{red,j}$ is the spectral interval of reduction used by the discretization group j. The resulting reduced spectrum is then obtained by combining $C_{\eta,red,j}$ and $\eta_{red,j}$ of each discretization group j.

The discretization schemes presented in this study should result in a more accurate approximation than an uniform reduction, such as the ones employed in [23], [24], as they allow variable levels of reduction depending on the importance of each band. In fact, the direct spectral integration (DSI) [23], [24] can be seen as a particular case of the SRI, where there is only one discretization group that employs the same reduction sample for the whole spectral contribution range of $0 \leq \zeta^*_{red} \leq 1$. At this point, it is not clear how to precisely define what level of spectral discretization each range of ζ^*_{red} requires for optimum balance between accuracy and computational cost of the solution. Furthermore, it is also not well understood what would be an adequate range of ζ^*_{red} for each discretization group j. The problem of how to satisfactorily define the discretization groups is addressed through testing different configurations in the results section.

As a starting point, five discretization schemes S1 to S5, each employing five discretization groups, are defined as shown in Table 1. For instance, the first scheme S1 divides these five discretization groups into uniform intervals of ζ^*_{red}, with the first group 1 ranging from $0.8 < \zeta^*_{red} \leq 1$ and employing a reduction sample $n_{red,1} = 1$ since these are the bands which contribute the most to the radiative transfer. As such, all the schemes proposed in the present study place the most important bands in the discretization group 1, which, consequently, always has the upper limit $\zeta^*_0 = 1$,, while the lower boundary ζ^*_1 varies from scheme to scheme. On the other hand, the last discretization group 5 from all these initially proposed schemes consider the lower limit of $\zeta^*_5 = 0$. The other intermediate discretization groups j range from $\zeta^*_j < \zeta^*_{red} \leq \zeta^*_{j-1}$, where both ζ^*_j and ζ^*_{j-1} also vary from scheme to scheme.

Table 1. Upper and lower limits of the five discretization groups from the initially proposed schemes S1 to S5

Scheme	ζ_0^*	ζ_1^*	ζ_2^*	ζ_3^*	ζ_4^*	ζ_5^*
S1	1	0.8	0.6	0.4	0.2	0
S2	1	0.5	0.3	0.2	0.1	0
S3	1	0.4	0.2	0.1	0.05	0
S4	1	0.3	0.15	0.05	0.02	0
S5	1	0.2	0.1	0.05	0.02	0

The data from Table 1 also shows that the schemes start from a uniform division of ζ_{red}^* in S1 and shift to a more non-uniform approach as the schemes go from S2 to S5, assigning a broader range of ζ_{red}^* to the discretization group 1, which employs the finest discretization. Consequently, the range of the less refined discretization groups 2-4 decrease from S1 to S5. The idea behind these configurations is to start from a more ambitious reduction scheme S1, in the sense that it only implements the finest discretization in the very high contributions from $0.8 < \zeta_{red}^* \leq 1$, and then move to a more conservative scheme S5, which assumes that the whole range from $0.2 < \zeta_{red}^* \leq 1$ requires the most refined spectral intervals. One should, therefore, expect that the most conservatives schemes S4 and S5 are able to generate more accurate solutions than S1.

Since the spectral contributions $\zeta_{q_r,red}^*$ and $\zeta_{S_r,red}^*$ are slightly different from each other, as can be seen in Fig. 3, defining discretization groups based on one or the other would result in distinct spectral intervals. Thus, the proposed schemes could either be based on the radiative heat flux, source term, or both. It is expected that the schemes based solely on either the radiative heat flux or source term would be optimal when that specific quantity is of greater interest, while schemes based on both would be more reliable when both quantities are important, yet probably at the cost of a higher total number of spectral intervals. When the methodology is based on the spectral contributions to both the radiative heat flux and source term, the discretization groups obtained for each quantity are compared and the one which requires the highest discretization becomes the final discretization group.

A visual representation of how the boundaries ζ_j^* from both schemes S1 and S5 compare to the spectral contributions to the radiative heat flux in the first example is presented in Fig. 4. The figure highlights the significant differences from the boundaries ζ_j^* of both schemes, contrasting the uniform division of the discretization groups of S1 to the highly non-uniform division in S5. When comparing the discretization group 1 from both schemes, there is only a very narrow band near 2150 cm^{-1} that is included in this most refined group, while S5 presents several regions between 1000 cm^{-1} to 2300 cm^{-1} and 3000 cm^{-1} to 4100 cm^{-1} in this same group. In fact, the discretization group 1 of S5 by itself has the same number of intervals as the S1 groups 2-4 combined. Furthermore, most of the bands in S1 fall within the discretization group 5, which should hinder significantly the accuracy of the SRI solution since this is the least important group for heat transfer. Despite these conclusions, if the solution of S1 is fast enough, it might still be an interesting scheme as it could present a good balance between accuracy and CPU cost.

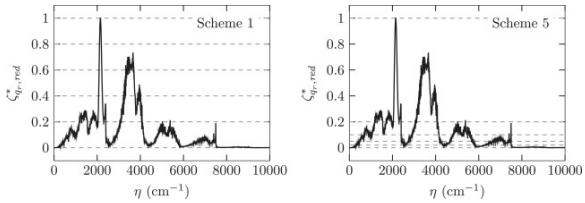

Fig. 4. Spectral contributions of the reduced bands to the radiative heat flux along with the discretization schemes S1 and S5 for the first example.

The same values of reduction samples $n_{red,j}$ are defined for all these initially proposed schemes S1 to S5. The idea behind this is that, by fixing $n_{red,j}$, the effect of the different chosen boundaries ζ_j^* is isolated, allowing a clearer conclusion on which are the most interesting division methods. Thus, the chosen values of $n_{red,j}$ for the discretization groups of schemes S1 to S5 are: $n_{red,1} = 1$, $n_{red,2} = 2$, $n_{red,3} = 5$, $n_{red,4} = 20$, $n_{red,5} = 100$. The selection of $n_{red,1} = 1$ for the first discretization group is justified by the initial idea that, in order to obtain accurate SRI solutions, the most important bands need to present the same spectral resolution as the reference LBL calculation. On the other hand, the reduction sample $n_{red} = 100$ of the last discretization group is equal to the $n_{red} = 100$, initially applied to the spectral contributions of the bands. This aims to guarantee that even a region composed of only one η_{red} point is able to be spectrally reduced. Other propositions can be attempted to optimize the discretization schemes, but it is expected that the present schemes will provide a good illustration of how to reduce the computational time of the LBL integration while keeping satisfactory accuracy.

Since the schemes are generated based on the spectral contributions of a certain case, their greatest limitation is that they require, at first, a previous reference LBL solution of the problem. To address that, this study proposes two different approaches. The first one is to employ discretizaton schemes based on a certain problem to solve other similar problems. The second one is to apply the reduction technique on the absorption cross-sections before the spectral contributions of the bands are calculated, which considerably reduces the CPU cost of this step.

3. Results and discussion

3.1. First analysis of the discretization schemes

For this first analysis, the chosen test case, named Case 2, consists of a homogeneous H_2O-CO_2 mixture at 1 atm, with $Y_w = 0.2$ and $Y_c = 0.1$, and temperatures varying from 300 K to 2500 K, such that

(21)

$$T = 300\text{K} + 2200\text{K}\sin^2(\pi x)$$

where the walls are 1 m apart from each other. The mole fractions are similar to what is observed in stoichiometric combustion of methane, which is the main application of interest in this study. Moreover, the temperature profile represents a flame with high temperature in the middle of the domain, around the reaction zone, and surrounded by cold walls in the boundaries, which are nearly at room temperature. A peak temperature of 2500 K is chosen to ensure that a critical condition is analyzed, even though methane flames usually do not reach such high values.

For these conditions of Case 2, the spectral contributions of the bands to the radiative heat flux and source term are presented in Fig. 5. According to this figure, the results of $\zeta_{q_r,red}^*$ and $\zeta_{S_r,red}^*$ resemble each other, but the few differences should result in slightly distinct discretization schemes and variations in terms of accuracy. As previously discussed in Section 2.4, it is expected that a discretization based on $\zeta_{q_r,red}^*$ results in better agreement for the radiative heat flux, while schemes based on $\zeta_{S_r,red}^*$ would favor the radiative source term. In order to verify if this hypothesis is correct, the next step of this analysis is to develop and compare various discretization schemes based on the spectral contributions to the radiative heat flux, radiative source term, and both for this homogeneous Case 2.

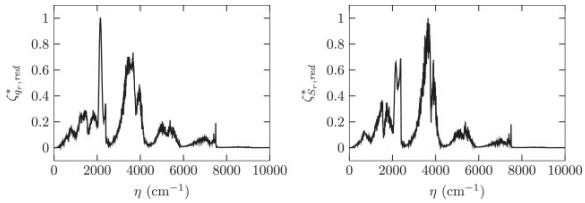

Fig. 5. Spectral contributions of the reduced bands to the radiative heat flux and source term for Case 2.

To start this analysis, the first schemes are developed based on the radiative heat flux. As can be seen in Fig. 5, the contributions $\zeta^*_{q_r,red}$ from the spectral band around 2150 cm^{-1} are the strongest, followed by the ones from the band near 3600 cm^{-1}. Every other region is considerably weaker, presenting $\zeta^*_{q_r,red} < 0.3$ even close to the peak located at 1440 cm^{-1}. It is therefore safe to infer that the initially proposed scheme S1 would not the best option to achieve high accuracy. Thus, schemes S2 to S5 would probably be more adequate, as they divide $\zeta^*_{q_r,red}$ in a non-uniform manner, placing a higher priority on the strongest bands.

When applying the discretization schemes S1 to S5 on the results of $\zeta^*_{q_r,red}$ from Fig. 5, the resulting numbers of spectral intervals are shown in Table 2. The data from the table shows that the total number of points $n_{p,t}$ increases considerably from schemes S1 to S5, especially in the first ones. Thus, the computational time also increases significantly, from almost 22 times faster than the reference for scheme S1 to slightly more than 3 times faster for S5. It is also interesting to notice that the number of elements $n_{p,t}$ from each discretization group of the same scheme goes from a more even distribution in S1 to a a high concentration in the groups 1 and 2 in S5, due to the higher priority placed on the strongest bands in this case.

Table 2. Number of spectral intervals from the discretizations schemes S1 to S5 based on q_r for Case 2.

Scheme	$n_{p,1}$	$n_{p,2}$	$n_{p,3}$	$n_{p,4}$	$n_{p,5}$	$n_{p,t}$
S1	1300	2400	1020	920	1204	6844
S2	8600	3450	2820	1230	958	17058
S3	11 200	9200	4920	1060	746	27 126
S4	15 500	10 700	7700	1220	502	35 622
S5	29 600	12 300	4240	1220	502	47 862

However, the higher computational cost of scheme S5 is compensated by the increase in accuracy. In fact, this can be seen in Fig. 6, which presents the comparison between the SRI using S1 and S5 to the reference LBL solution. These results show that the S5 solution, despite being more costly, is very close to the original LBL and could be used to generate benchmark solutions. On the other hand, the less refined S1 scheme leads to small deviations near the positive and negative peaks of both the radiative heat flux and source term, but could still be an adequate alternative for faster calculations that do not require benchmark levels of accuracy. One interesting conclusion that can be drawn from Fig. 6 is that, even though the discretization schemes were developed based on the radiative heat flux, the solutions for the radiative source term present similar deviations.

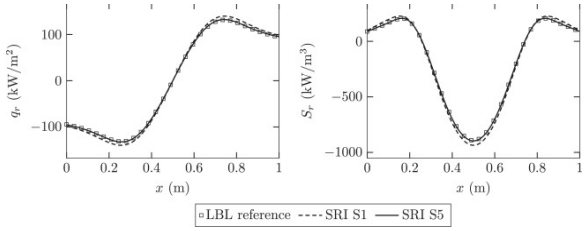

Fig. 6. Radiative heat flux and source term solutions from the reference LBL and the SRI using S1 and S5 for Case 2.

Similar analyses are also performed for the discretization schemes S1 to S5 based on the radiative source term and based on both the radiative heat flux and source term. Since the results of these other two methodologies are very similar to the one presented in Fig. 6, based on the radiative heat flux, they are omitted here. However, these other methodologies present slightly different ratios between accuracy and computational time. This particularity can be better understood in Fig. 7, which presents the average deviations of the radiative heat flux, $\delta_{q_r,avg}$, and source term, $\delta_{S_r,avg}$, as a function of the total number of spectral intervals for all the discretization schemes from this first study. The figure shows that all the three solutions behave similarly: as the total number of points $n_{p,t}$ increases, the average deviations of both quantities decrease, even though the radiative heat flux deviations are overall slightly higher. The gain in accuracy is more pronounced in the first schemes S1 to S3, but seem to slow down in the more refined schemes S4 and S5. Despite that, if highly accurate results are desired, the most refined schemes S4 and S5 are recommended.

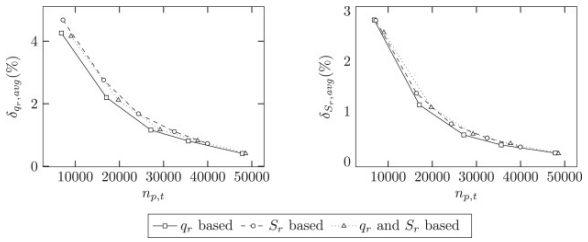

Fig. 7. Average deviations of the SRI solutions for radiative heat flux and source term with respect to the reference LBL for Case 2. The different discretization schemes S1 to S5 lead to different total numbers of spectral intervals.

To deepen the understanding of this first study, new schemes are attempted, but now fixing the reduction samples $n_{red,i}$ and varying ζ_i. The idea is to use the most refined scheme S5 as the starting point, fixing its bounds ζ_i, and increase $n_{red,i}$ to obtain faster solutions without significant increases in deviations. As previously discussed, if $n_{red,1} = 1$, which should be the ideal value if accuracy is desired, the number of points of the discretization group 1 is already dominant for all the methodologies, limiting the generation of more efficient schemes. Based on this, some of these new discretizations present $n_{red,1} > 1$ as an effort to obtain schemes as fast as S1 to S3, yet with better accuracy. The reduction samples $n_{red,i}$ and the resulting total number of points $n_{p,t}$ of the new schemes S6 to S8 for the three different methodologies, together with the ones from scheme S5, are presented in Table 3. This data also shows that the q_r based methods always present higher total number of points than the S_r based.

Table 3. Reduction samples and total number of points from the discretizations schemes S5 to S8 for Case 2.

						$n_{p,t}$		
Scheme	$n_{red,1}$	$n_{red,2}$	$n_{red,3}$	$n_{red,4}$	$n_{red,5}$	**q_r based**	**S_r based**	**q_r and S_r based**
S5	1	2	5	20	100	47 862	39 945	48 583
S6	1	5	20	50	100	36 570	30 921	37 417
S7	2	5	20	50	100	21 770	18 221	22 167
S8	3	10	50	100	100	13 398	11 331	13 670

To verify if the new schemes S6-S8 are adequate, Fig. 8 illustrates the average deviations of schemes S5 to S8, using all three methodologies, as a function of the total number of spectral intervals for this first study. This figure shows that, despite S8 employing high reduction samples than the others, it results in surprisingly low deviations when considering its amount of spectral intervals. In fact, S8 seems to have a better compromise

between accuracy and computational cost than S1. However, as the total number of points increases, the difference between the new schemes S6 to S8 and the previous S1 to S5 diminishes and the deviations seem to become more a function of the total number of points rather than the scheme configuration. Similarly to what was observed in Fig. 7, the radiative heat flux deviations are overall higher than the ones from the radiative source term, more than twice in some cases. On the other hand, the new schemes S6 to S8 present lower differences between the methodologies based on q_r, S_r, and both, except for $\delta_{q_r,avg}$ in the region from 19000 to 36000 points where the S_r based schemes perform worse than the others.

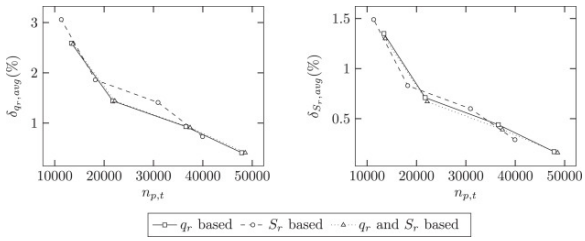

Fig. 8. Average deviations of the SRI solutions for radiative heat flux and source term with respect to the reference LBL for Case 2. The different discretization schemes S5 to S8 lead to different total numbers of spectral intervals.

With these last results, it can be concluded that the initial assumption that schemes based solely on the radiative heat flux or the radiative source term would result in more efficient solutions for the respective physical quantity is not necessarily true. Actually, it is really hard to define whether the schemes should be based on the spectral contributions to the radiative heat flux, source term or both, as their performance varies from scheme to scheme. Nonetheless, the differences between these methodologies are overall very small, which makes any of them a good alternative for generating discretization schemes, at least for this first study. Despite that, for new cases where such an in depth comparison is not performed, it is probably safer to account for the spectral contributions of both quantities. Therefore, for the next test cases, the schemes will only be based on both q_r and S_r. Among all the tested schemes, S4 and S8 are the ones chosen for the next calculations. The choice of S4 aims to provide very accurate results yet still maintain a good CPU time reduction, while S8 is a good alternative for a faster solution that still retains good compromise between deviations and total number of spectral intervals.

3.2. Non-homogeneous test cases

The test cases presented in this section involve non-uniform temperature and species concentration profiles that also aim to resemble stoichiometric combustion of methane in air at atmospheric total pressure. All these profiles consider a hot non-homogeneous gas medium, surrounded by cold black walls near room temperature that are 1 m apart from each other. Since this study is focused on combustion applications, despite the profiles varying from case to case, the temperature and mole fraction peaks always coincide somewhere in the gas mixture, which represents the flame main reaction zone where H_2O and CO_2 are being generated. Furthermore, all the species concentration profiles present a constant mole ratio $M_r = Y_w/Y_c = 2$ between them.

The first non-homogeneous test case, Case 3, employs the same temperature profile as the one introduced in Eq. (21), while Y_w and Y_c are given by

(22)

$$Y_w = 2Y_c = 0.2\sin^2(\pi x)$$

These profiles present their peak values in the middle of the domain, representing a single main reaction zone there. The second non-homogeneous test case, Case 4, employs a similar temperature profile as the one in Eq. (21), but now only going up to 1800 K, such that

(23)

$$T = 300\text{K} + 1500\text{K}\sin^2(\pi x)$$

which would be closer to temperatures of real methane flames in air-fuel combustion conditions. On the other hand, the species concentration profiles of Case 4 are the same as the ones from Case 3, shown in Eq. (22). The last test case consists of a non-homogeneous mixture where the temperature still ranges from 300 K to 1800 K like Case 4, but now with two temperature peaks, given by

(24)

$$T = \begin{cases} 300\text{K} + 1500\text{K}\sin^2(2\pi x) & \text{if } x \leq 0.25\text{m} \text{or} x > 0.75\text{m} \\ 1050\text{K} + 750\text{K}\sin^2(2\pi x) & \text{if } 0.25\text{m} < x \leq 0.75\text{m} \end{cases}$$

Since these peaks represent the main combustion reaction zone, the mole fraction profile of Case 5 also presents two maximum values in these same positions, such that

(25)

$$Y_c = \begin{cases} 0.1\sin^2(2\pi x) & \text{if} x \leq 0.25\text{m} \text{or} x > 0.75\text{m} \\ 0.05 + 0.05\sin^2(2\pi x) & \text{if} 0.25\text{m} < x \leq 0.75\text{m} \end{cases}$$

These last temperature and mole fraction profiles aim to represent the characteristic behavior along the radial axis in a flame, where there are two boundaries of the reaction zone. A better comparison between the profiles of each non-uniform test case is illustrated in Fig. 9, evidencing that Case 4 is basically a variation of Case 3, but with lower peak temperature, while Case 5 presents more significant variations.

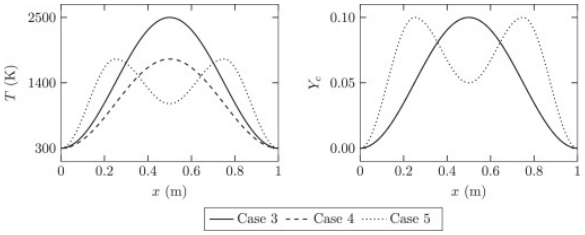

Fig. 9. Temperature and mole fraction profiles considered in Cases 3 to 5. The mole fractions Y_c from Cases 3 and 4 coincide along the domain.

For the conditions of Cases 3 to 5, the spectral contributions ζ^*_{red,q_r} and ζ^*_{red,S_r} are shown in Fig. 10. Surprisingly, these results show that there are only small variations between ζ^*_{red} of these test cases, despite their non-negligible differences in configuration, especially between Cases 3 and 5. When comparing Cases 3 to 4, it is seen that the contributions of the first bands become stronger in Case 4, especially to the radiative source term. The contributions of the later bands to both quantities are also weaker in Case 4, which is probably due to the Planck's distribution shift caused by the lower temperature peak. A similar conclusion is drawn when comparing the spectral contributions from Case 5 to those from Case 3, yet it is interesting to notice that ζ^*_{red,S_r} in Case 5 are overall lower than those observed in Case 4. However, despite these small differences, the similarities

between the ζ^*_{red} distributions might be enough for the schemes based on one solution to be applicable to the other.

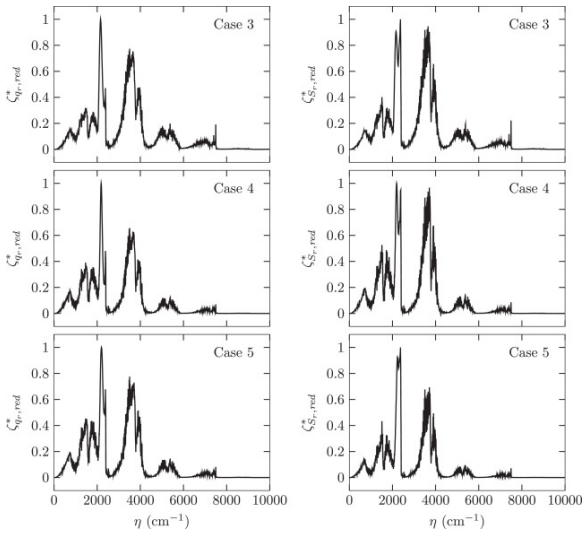

Fig. 10. Spectral contributions of the reduced bands to the radiative heat flux and source term for Cases 3 to 5.

The results for the SRI using both S4 and S8 and comparing them to the reference LBL are illustrated in Fig. 11. According to this figure, the scheme S4 is able to reproduce solutions with benchmark levels of accuracy in all three test cases, similar to what is concluded in the first study, despite the non-homogeneous conditions of the mixtures. The less refined scheme S8 also provides satisfactory accuracy when considering its low computational cost, making it a good alternative for faster solutions that require less accuracy. Overall, both schemes are successful, each in its own merit, showing that the methodology developed in this study is a good alternative to reduce the CPU time of the LBL even in non-homogeneous conditions.

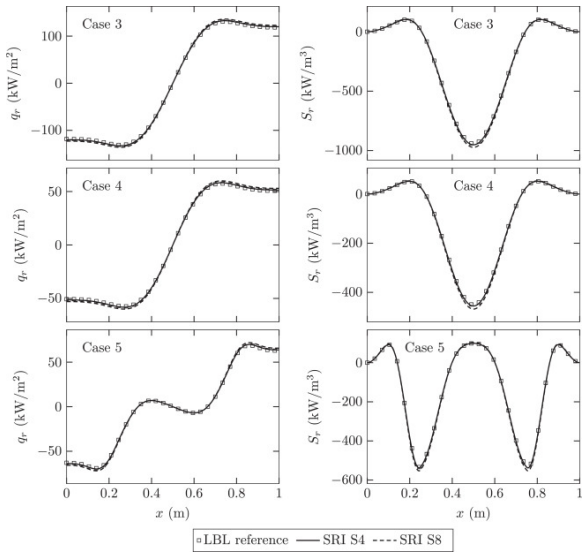

Fig. 11. Radiative heat flux and source term solutions from the reference LBL and the SRI using S4 and S8 for Cases 3 to 5.

In order to have a better grasp on the performance of the discretization schemes in each of these three scenarios, the average and maximum deviations of schemes S4 and S8, together with their resulting total number of points, are presented in Table 4 for Cases 3 to 5. This data shows that, for all the studied schemes,

the average deviations of the radiative heat flux are higher than the radiative source term ones, usually by a factor of 2 or more. Since this trend was also observed in Figs. 7 and 8, it is reasonable to assume that the proposed methodology results in higher average deviations for the radiative heat flux, at least when analyzing conditions similar to the ones from this study. However, it is interesting to notice that the maximum deviations of the radiative heat flux are not much higher than the ones from the radiative source term. For example, the variations of schemes S8 from Table 4 present radiative heat flux average deviations around 3%, which might not appear so impressive, but the maximum deviations are near 4%, a value that is not so easily attainable by other simpler gas models. Depending on the application, the maximum deviations might be a more important restriction than the average ones. In fact, this relatively low maximum deviations can be seen as one of the advantages of the SRI.

Table 4. Average and maximum deviations of the SRI using S4 and S8 for the radiative heat flux and source term with respect to the reference LBL for Cases 3 to 5.

Test case	**Scheme**	$\boldsymbol{n_{p,t}}$	$\delta_{q_r,avg}$	$\delta_{S_r,avg}$	$\delta_{q_r,max}$	$\delta_{S_r,max}$
Case 3	S4	35737	0.98	0.37	1.26	0.96
	S8	13028	3.01	1.18	3.83	3.25
Case 4	S4	33419	1.06	0.34	1.32	1.05
	S8	11619	3.52	1.22	4.38	3.84
Case 5	S4	35110	0.67	0.33	1.25	0.81
	S8	12190	2.21	1.36	4.30	3.61

When comparing the two different schemes in all cases, S8 presents a total number of points almost three times lower than S4, but at the cost of approximately three times higher deviations. Nonetheless, the accuracy from S8 is still competitive with other spectral models, being an interesting alternative for faster calculations. On the other hand, S4 is able to generate maximum deviations near 1 % and, thus, can be used to generate very accurate solutions almost five times faster than the reference LBL in all three cases. It is noted that the number of points resulted from the non-uniform cases are slightly lower than the ones reported in Table 3 for the first study. One possible reason for this is that the homogeneous medium present higher species concentrations on the lower temperature regions, which might increase the number of spectral intervals that contribute significantly. This would not be the case in combustion applications though.

3.2.1. Employing the same schemes between different cases

Despite the promising results of the SRI method in the previous sections, the analysis of the spectral contributions of the bands still have the limitation of requiring a previous reference LBL solution of the problem. As an attempt to address this issue, the first proposed methodology of employing schemes based on similar cases is tested by using the schemes S4 and S8 generated for Case 3 to solve Cases 4 and 5. The results of such analysis are illustrated in Fig. 12, again comparing the SRI solutions with the reference LBL. To differentiate them from the schemes S4 and S8 from the original methodology, these schemes based on Case 3 are named, respectively, $S4_{C3}$ and $S8_{C3}$. The figure shows that the schemes based on Case 3 provide surprisingly accurate results for both Cases 4 and 5, which are comparable to the ones obtained from the original schemes based on them. When looking at the numerical values of the deviations in Table 5, it is noteworthy that the schemes $S4_{C3}$ and $S8_{C3}$ resulted in Cases 4 and 5 solutions as accurate, and sometimes even more accurate, than the schemes S4 and S8 developed based on their own ζ_{red}^* distributions. The probable reason for this is that, despite the schemes $S4_{C3}$ and $S8_{C3}$ having the downside of not considering the best ζ_{red}^* distributions, they result in a discretization with higher total number of points $n_{p,t}$, compensating for the differences between the test cases. However, the main reason for this good agreement is still mainly due to the similarity between the ζ_{red}^* distributions of the involved test cases, shown in Fig. 10.

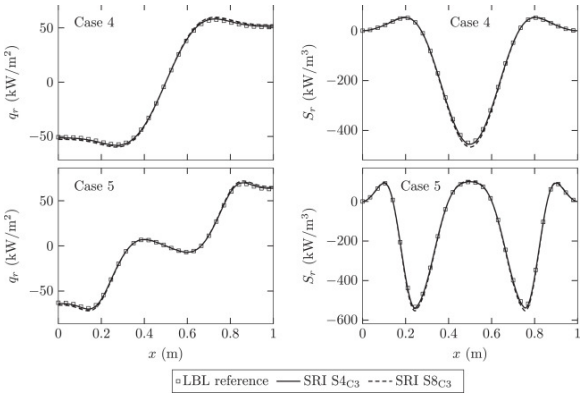

Fig. 12. Radiative heat flux and source term solutions from the reference LBL and the SRI using $S4_{C3}$ and $S8_{C3}$ for Cases 4 and 5.

Table 5. Average and maximum deviations of the SRI using $S4_{C3}$ and $S8_{C3}$ for the radiative heat flux and source term with respect to the reference LBL for Cases 4 and 5.

Test case	**Scheme**	$\boldsymbol{n_{p,t}}$	$\delta_{q_r,avg}$	$\delta_{S_r,avg}$	$\delta_{q_r,max}$	$\delta_{S_r,max}$
Case 4	$S4_{C3}$	35737	0.97	0.34	1.22	0.97
	$S8_{C3}$	13028	3.20	1.16	4.04	3.50
Case 5	$S4_{C3}$	35737	0.66	0.38	1.28	0.92
	$S8_{C3}$	13028	2.14	1.40	4.20	3.61

The good performance of this methodology is especially interesting in Case 5, which has considerably different configuration than Case 3. The only characteristics that these problems have in common are: cold walls at 300 K with a hot medium in between them and the constant mole ratio of the species $M_r = Y_w/Y_c = 2$ along the whole domain. In particular, the similarity in mole ratio might have a high influence on this good agreement since identical M_r means that the ratio between the importance of the absorption spectra of H_2O and CO_2 remains the same in both cases. Independent studies, not presented here for brevity, showed that even if both Y_w and Y_c varies, the methodology is still applicable as long the mole ratio remains $M_r = 2$. However, if M_r varies considerably, the accuracy of the methodology is hindered. For example, these tests showed that when schemes $S4_{C3}$ and $S8_{C3}$ were used to solve a problem similar to Case 5 yet with different M_r, the results remained accurate while $1.8 \leq M_r \leq 2.2$, but deviations became more significant for increasingly distant M_r values. Other independent studies also showed that if the walls are hot and the medium is cold, the spectral contributions change considerably and, therefore, using schemes developed for cold walls and hot medium would not be advisable. Nonetheless, since most combustion scenarios consist of a hot medium bounded by cold walls, this should not be a significant issue.

Despite these limitations, the conclusion of this analysis is that schemes developed for a certain case (e.g. Case 3) could be used to accurately solve another one with considerably different configuration (e.g. Case 5), as long as they present basic similarities. This means that new users of the methodology do not necessarily need to obtain a reference LBL calculation, which might be very CPU time intensive, and could instead use discretization schemes that were previously developed by other authors or for simpler problems. For instance, the user could first solve the decoupled combustion problem, find the mole fraction and temperature profiles, and, as long as the decoupled solution is sufficiently similar, use them to generate SRI schemes to solve the coupled problem. Regarding the degree of similarity needed between the cases, it is recommended that both present the same relation between walls and medium (e.g. cold walls and hot medium) and similar M_r between species, at least in

the regions that are most important to radiative transfer. However, further testing of these requirements might be a topic of interest for future studies.

3.2.2. Generation of spectral contributions from previously reduced spectra

If schemes that were previously generated for similar cases are not available, the spectral contributions of the bands need to calculated before the use of the SRI method. On the results presented up to this point, the ζ^* distributions are first generated from the reference resolution spectrum with $\Delta\eta = 0.0667\ \mathrm{cm}^{-1}$ and then spectrally reduced by $n_{red} = 100$,. The idea behind this procedure is to minimize the deviations caused by the spectral reduction by applying it only on the final results of interest. However, since the spectral contributions need to be reduced anyway, as previously discussed, this technique could be employed in the absorption spectrum from which the ζ^* distributions are calculated instead. In this case, the methodology would be analogous to the one utilized by [23], but limited only to the development of the discretization schemes. This should considerably reduce the computational time of generating the spectral contributions, but should also lower the accuracy of the resulting schemes.

To verify this assumption, the initial absorption cross-section used to generate the spectral contributions of Case 5 were initially reduced by samples of $n_{red} = 100$, 1000 and 10 000. The choice of Case 5 for this analysis is based on the possibility of comparing this methodology to the one employing schemes from similar cases, where Case 5 is successfully solved using $S4_{C3}$ and $S8_{C3}$, as can be seen in Fig. 12. When the schemes S4 and S8 are developed based on Case 5 and using this new technique with the three proposed reduction samples, the results of the SRI method are shown in Fig. 13. According to this figure, the performance of this new methodology was surprisingly good, even for the least refined absorption spectrum using nred=10000. In fact, if only the results from Fig. 13 are taken into account, applying the highest spectral reduction seems like the best alternative since the evaluation of the spectral contributions are approximately 100 times faster than the schemes considering $n_{red} = 100$, with minimal losses in accuracy.

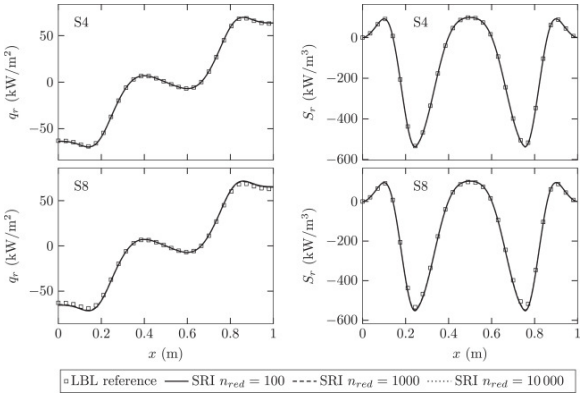

Fig. 13. Radiative heat flux and source term solutions of Case 5 from the reference LBL and the SRI using the schemes S4 and S8 with different initial reductions.

Nonetheless, despite this gain in pre-processing, the discretization schemes generated from these coarser ζ^* distributions ended up presenting a higher total number of points, which are shown in Table 6 together with the deviations from each of the analyzed schemes. This table illustrates that even the lowest initial reduction of $n_{red} = 100$ still resulted in a higher $n_{p,t}$ than the ones presented in Table 4 for both the original Case 5 schemes. Independent studies indicated that this was caused by the fact that spectrally reduced absorption spectra resulted in ζ^* distributions higher than the ones calculated based on the original spectra. This overestimation in the spectral contributions of the bands leaded to more conservative schemes with higher total of points, which increased with the initial n_{red}. It also is interesting to notice that, if Table 4 and 6 are compared, this new methodology resulted in deviations lower than the ones from the original Case 5 schemes. This is

probably a consequence of the higher amount of spectral intervals, which compensated for the loss in accuracy caused by the spectrally reduced absorption cross-sections. An example of this effect can be noticed on the increase in accuracy from $n_{red} = 100$ to $n_{red} = 1000$.

Table 6. Average and maximum deviations for the solutions of Case 5 for the discretization schemes S4 and S8 with different initial reductions.

Scheme	n_{red}	$n_{p,t}$	$\delta_{q_r,avg}$	$\delta_{S_r,avg}$	$\delta_{q_r,max}$	$\delta_{S_r,max}$
S4	100	38 711	0.49	0.24	0.91	0.59
	1000	41 010	0.46	0.23	0.87	0.56
	10 000	52 500	0.55	0.35	1.10	0.92
S8	100	13 116	2.01	1.30	3.94	3.44
	1000	14 212	1.64	1.09	3.23	2.89
	10 000	15 632	2.05	1.34	4.03	3.49

The conclusion from the results of Fig. 13 and Table 6 is that the methodology of generating spectral contributions from previously reduced spectra is a good alternative to address the main limitation of the SRI model. In fact, the performance of this approach is comparable to the one which employs schemes based on similar cases, yet with the advantage that it does not require specific previously generated solutions. However, even with spectrally reduced absorption cross-sections, the generation of ζ^* distributions could still be considered a drawback, especially when solving coupled problems. It would still be a great advantage to develop the discretizations schemes based on the decoupled solution, as long as it is sufficiently similar, and then use them to obtain the coupled solution. In such case, the two different proposed methodologies could be used together to reduce even further the CPU time of the schemes pre-processing.

4. Conclusions

This study presented a new methodology of spectral integration for the solution of the RTE, the spectrally reduced integration (SRI), which was based on the spectral contributions of the bands to the radiative heat flux and source term. The SRI utilizes these spectral contributions to generate reliable non-uniform discretization schemes that are able to considerably reduce the number of spectral intervals in the RTE integration while still maintaining accurate solutions. A total of eight different discretization schemes, S1 to S8, were generated and tested for both homogeneous and non-homogeneous mixtures of H_2O and CO_2.

Since the spectral contributions can be based on the radiative heat flux, the radiative source term, or both, these three approaches were tested for a homogeneous mixture test case. However, results showed that the differences between them, in terms of accuracy and computational cost, were very small. This test case also made it clear that the accuracy of the SRI method continuously increased with the total number of points, but there were diminishing returns as the discretization schemes became finer. The most refined schemes S4 and S5 presented average deviations lower than 1%, which could be regarded as benchmark levels of accuracy, with solution speeds 3 to 5 times faster than the reference LBL. Furthermore, S8 stood out as a good alternative for faster calculations.

For the non-uniform test cases, similar conclusion were obtained: S4 was again able to generate average deviations lower than 1% almost 5 times faster than the reference LBL while the coarser scheme S8 resulted in even faster solutions, at the cost of slightly higher deviations. Moreover, these non-uniform cases were also used to verify the performance of two proposed methodologies to address the need of a prior evaluation of the spectral contributions from LBL reference solutions: one which employs discretization schemes based on a similar problem and the other which generates spectral contributions from significantly coarser LBL solutions.

Both approaches performed surprisingly well in the conditions studied in this study, providing similar levels of accuracy as the original methodology of the SRI, and could be used together to make the method's applicability even broader. Nonetheless, results also showed that, to obtain such agreement, some considerations should be acknowledged before employing them.

In summary, this study showed that the SRI is a good alternative to obtain benchmark solutions when LBL calculations are prohibitive, with deviations considerably lower than the alternative method proposed by Ziemniczak et al. [23]. When compared to narrow-band models, the SRI is a more computational costly methodology, at least in atmospheric total pressure applications, but has the advantage of allowing discretization schemes as refined as the user desires. In high total pressure conditions, due to the smoothing of the absorption spectra [9], [10], the LBL requires a considerably lower spectral resolution, which could make the SRI even more competitive. Therefore, extending the SRI to higher total pressures and comparing to narrow-band models is a good direction for further studies. Although this study is limited to 1D test cases, preliminary results show that the methodology is also applicable to 2D and 3D problems, so adapting the SRI to multidimensional scenarios is also an important next step in this research.

Declaration of Competing Interest

These sources are adequately mentioned in the Acknowledgments section of the manuscript. None of the authors presently have or have had in the past any financial relationships that may compromise the integrity of this work.

Acknowledgments

This study was financed in part by the Coordenação de Aperfeiçoamento de Pessoal de Nível Superior - Brasil (CAPES) - Finance Code 001. Author FHRF also thanks CNPq (Brazil) for research grants 302686/2017-7.

References

[1] M.F. Modest. **Radiative Heat Transfer.** Academic Press (2013)

[2] M.F. Modest, D.C. Haworth. **Radiative Heat Transfer in Turbulent Combustion Systems: Theory and Applications.** Springer (2016)

[3] J.R. Howell, M.P. Mengüç, R. Siegel. **Thermal Radiation Heat Transfer.** (6th), CRC press (2016)

[4] A. Soufiani, J. Taine. **High temperature gas radiative property parameters of statistical narrow-band model for H_2O, CO_2 and CO, and correlated-k model for H_2O and CO_2.** Int. J. Heat Mass Transf., 40 (4) (1997), pp. 987-991, 10.1016/0017-9310(96)00129-9

[5] P. Rivière, A. Soufiani. **Updated band model parameters for H_2O, CO_2, CH_4 and CO radiation at high temperature.** Int. J. Heat Mass Transf., 55 (13-14) (2012), pp. 3349-3358, 10.1016/j.ijheatmasstransfer.2012.03.019

[6] J. Cai, M.F. Modest. **Improved full-spectrum k-distribution implementation for inhomogeneous media using a narrow-band database.** J. Quant. Spectrosc. Radiat. Transf., 141 (2014), pp. 65-72, 10.1016/j.jqsrt.2014.02.028

[7] L.J. Dorigon, G. Duciak, R. Brittes, F. Cassol, M. Galarça, F.H. França. **WSGG correlations based on HITEMP2010 for computation of thermal radiation in non-isothermal, non-homogeneous H_2O/CO_2 mixtures.** Int. J. Heat Mass Transf., 64 (2013), pp. 863-873, 10.1016/j.ijheatmasstransfer.2013.05.010

[8] M.H. Bordbar, G. Węcel, T. Hyppänen. **A line by line based weighted sum of gray gases model for inhomogeneous CO_2–H_2O mixture in oxy-fired combustion.** Combust. Flame, 161 (9) (2014), pp. 2435-2445, 10.1016/j.combustflame.2014.03.013

[9] F.R. Coelho, F.H. França. **WSGG correlations based on HITEMP2010 for gas mixtures of H_2O and CO_2 in high total pressure conditions.** Int. J. Heat Mass Transf., 127 (2018), pp. 105-114, 10.1016/j.ijheatmasstransfer.2018.07.075

[10] J.T. Pearson, B.W. Webb, V.P. Solovjov, J. Ma. **Effect of total pressure on the absorption line blackbody distribution function and radiative transfer in H_2O, CO_2, and ceCO.** J. Quant. Spectrosc. Radiat. Transf., 143 (2014), pp. 100-110, 10.1016/j.jqsrt.2013.08.011

[11] V.P. Solovjov, F. Andre, D. Lemonnier, B.W. Webb. **The rank correlated SLW model of gas radiation in non-uniform media.** J. Quant. Spectrosc. Radiat. Transf., 197 (2017), pp. 26-44, 10.1016/j.jqsrt.2017.01.034

[12] M.F. Modest, H. Zhang. **The full-spectrum correlated-k distribution and its relationship to the weighted-sum-of-gray-gases method.** Proceedings of IMECE2000 (2000)

[13] H. Zhang, M.F. Modest. **A multi-scale full-spectrum correlated-k distribution for radiative heat transfer in inhomogeneous gas mixtures.** J. Quant. Spectrosc. Radiat. Transf., 73 (2-5) (2002), pp. 349-360, 10.1016/s0022-4073(01)00220-5

[14] M.F. Modest, R.J. Riazzi. **Assembly of full-spectrum k-distributions from a narrow-band database effects of mixing gases, gases and nongray absorbing particles, and mixtures with nongray scatterers in nongray enclosures.** J. Quant. Spectrosc. Radiat. Transf., 90 (2) (2005), pp. 169-189, 10.1016/j.jqsrt.2004.03.007

[15] H. Chu, M. Gu, J.-L. Consalvi, F. Liu, H. Zhou. **Effects of total pressure on non-grey gas radiation transfer in oxy-fuel combustion using the LBL, SNB, SNBCK, WSGG, and FSCK methods.** J. Quant. Spectrosc. Radiat. Transf., 172 (2016), pp. 24-35

[16] J. Consalvi, F. Andre, F. Coelho, F. Franca, F. Nmira, M. Galtier, V. Solovjov, B. Webb. **Assessment of engineering gas radiative property models in high pressure turbulent jet diffusion flames.** J. Quant. Spectrosc. Radiat. Transf., 253 (2020), p. 107169, 10.1016/j.jqsrt.2020.107169

[17] G.N. Schenker, B. Keller. **Line-by-line calculations of the absorption of infrared radiation by water vapor in a box-shaped enclosure filled with humid air.** Int. J. Heat Mass Transf., 38 (17) (1995), pp. 3127-3134, 10.1016/0017-9310(95)00098-t

[18] S. Chauveau, C. Deron, M.-Y. Perrin, P. Rivière, A. Soufiani. **Radiative transfer in LTE air plasmas for temperatures up to 15,000 K.** J. Quant. Spectrosc. Radiat. Transf., 77 (2) (2003), pp. 113-130, 10.1016/s0022-4073(02)00080-8

[19] K. Beier, E. Lindermeir. **Comparison of line-by-line and molecular band IR modeling of high altitude missile plume.** J. Quant. Spectrosc. Radiat. Transf., 105 (1) (2007), pp. 111-127, 10.1016/j.jqsrt.2006.09.019

[20] H. Chu, F. Liu, H. Zhou. **Calculations of gas thermal radiation transfer in one-dimensional planar enclosure using LBL and SNB models.** Int. J. Heat Mass Transf., 54 (21-22) (2011), pp. 4736-4745

[21] H. Chu, J.-L. Consalvi, M. Gu, F. Liu. **Calculations of radiative heat transfer in an axisymmetric jet diffusion flame at elevated pressures using different gas radiation models.** J. Quant. Spectrosc. Radiat. Transf., 197 (2017), pp. 12-25, 10.1016/j.jqsrt.2017.02.008

[22] A. Wang, M.F. Modest. **Importance of combined Lorentz-Doppler broadening in high-temperature radiative heat transfer applications.** J. Heat Transf., 126 (5) (2004), p. 858, 10.1115/1.1798951

[23] A. Ziemniczak, F.R. Coelho, F.M. Pereira, P.R. Pagot, F.H.R. França. **Evaluation of the discretization in the spectral resolution for the solution of the line-by-line method in problems with participating gases.** J. Brazil. Soc. Mech. Sci. Eng., 41 (9) (2019), 10.1007/s40430-019-1855-z

[24] L.G.P. Rodrigues, I.M. Machado, A. Ziemniczak, F.M. Pereira, P.R. Pagot, F.H.R. França. **Comparisons between numerical simulations and experimental measurements of radiative heat flux for a series of CH_4/N_2 diluted laminar non-premixed flames.** Combust. Sci. Technol. (2019), pp. 1-22

[25] A. Wang, M.F. Modest. **Spectral Monte Carlo models for nongray radiation analyses in inhomogeneous participating media.** Int. J. Heat Mass Transf., 50 (19-20) (2007), pp. 3877-3889, 10.1016/j.ijheatmasstransfer.2007.02.018

[26] T. Ozawa, M.F. Modest, D.A. Levin. **Spectral module for photon Monte Carlo calculations in hypersonic nonequilibrium radiation.** J. Heat Transf., 132 (2) (2010), p. 023406, 10.1115/1.4000242

[27] A. Feldick, M.F. Modest. **An improved wavelength selection scheme for Monte Carlo solvers applied to hypersonic plasmas.** J. Quant. Spectrosc. Radiat. Transf., 112 (8) (2011), pp. 1394-1401, 10.1016/j.jqsrt.2011.01.028

[28] T. Ren, M.F. Modest. **A hybrid wavenumber selection scheme for line-by-line photon Monte Carlo simulations in high-temperature gases.** J. Heat Transf., 135 (8) (2013), p. 084501, 10.1115/1.4024385

[29] T. Ren, M.F. Modest, S. Roy. **Monte Carlo simulation for radiative transfer in a high-pressure industrial gas turbine combustion chamber.** J. Eng. Gas Turbin. Power, 140 (5) (2017), p. 051503, 10.1115/1.4038153

[30] S.P. Roy, J. Cai, M.F. Modest. **Development of a multiphase photon Monte Carlo method for spray combustion and its application in high-pressure conditions.** Int. J. Heat Mass Transf., 115 (2017), pp. 453-466, 10.1016/j.ijheatmasstransfer.2017.07.046

[31] T. Ren, M.F. Modest. **Line-by-line random-number database for Monte Carlo simulations of radiation in combustion system.** J. Heat Transf., 141 (2) (2018), p. 022701, 10.1115/1.4041803

[32] J.T. Pearson, B.W. Webb, V.P. Solovjov, J. Ma. **Efficient representation of the absorption line blackbody distribution function for H_2O, CO_2, and CO at variable temperature, mole fraction, and total pressure.** J. Quant. Spectrosc. Radiat. Transf., 138 (2014), pp. 82-96

[33] Rothman, I. Gordon, R. Barber, H. Dothe, R. Gamache, A. Goldman, V. Perevalov, S. Tashkun, J. Tennyson. **HITEMP, the high-temperature molecular spectroscopic database.** J. Quant. Spectrosc. Radiat. Transf., 111 (15) (2010), pp. 2139-2150, 10.1016/j.jqsrt.2010.05.001

[34] F. Cassol, R. Brittes, F.H. França, O.A. Ezekoye. **Application of the weighted-sum-of-gray-gases model for media composed of arbitrary concentrations of H_2O, CO_2 and soot.** Int. J. Heat Mass Transf., 79 (2014), pp. 796-806, 10.1016/j.ijheatmasstransfer.2014.08.032